Simulation-based Analysis of the Effects of Feedwater Distribution on Vapor Hold-up in Kettle-type Waste Heat Boilers

E. Nasato[1], T. Treeratanaphitak[2], and N.M. Abukhdeir[3*]

[1]Nasato Consulting Ltd., Oakville, Ontario, Canada
[2]Sirindhorn International Institute of Technology, Thammasat University
Pathum Thani, Thailand
[3]Continuum Engineering Inc.
Waterloo, Ontario, Canada

Presented at the 30th Annual Brimstone Sulfur Recovery Symposium
Vail Colorado September 11, 2023

Introduction

Waste heat boilers (WHBs) are an important component of the sulfur recovery unit (SRU) where energy generated from desulfurization of feed gas, predominantly using some variation of the Claus process, is recovered for upstream use. Modern WHBs are designed for the generation of significantly higher pressure steam than in the past, along with existing legacy units being retrofitted for higher heat loads and operating pressures. Both the design of "clean-sheet" WHBs and retrofit of legacy units poses increased technical challenges, which has resulted in increasing numbers of operating deviations and failures [1]. These failures are especially pronounced in kettle-type WHBs due to the complex shell-side multiphase hydrodynamics present which are not well understood. This is especially the case within and around the tube bundle in which the competition between convective mass transfer (liquid and vapor) and phase change (boiling) occurs [2]. Compared to thermosiphon-type units, in which recirculation is inherently simplified through their design, typical kettle-type WHBs are limited to a single feed water inlet and a single steam outlet. Thus recirculation occurs within the shell-side, where a liquid/vapor interface is present, compared to the modular thermosiphon design with recirculation imposed through the use of a separate steam drum and multitude of risers and downcomers.

In the majority of kettle-type WHB designs, feedwater is injected through a single inlet and redirected using a simple deflection plate. However, the heat flux within the submerged tube bundle varies both radially and axially, with axial variation being greatest due to the large decrease in temperature of the process gas within the inlet region. Figure 1a shows a schematic of the average heat flux versus temperature for a typical industrial scale WHB based on semi-empirical models used for design (for both standard and oxygen-enrichment operating conditions). Thus a single injection point of feedwater is intuitively not ideal and, instead, feedwater should be distributed throughout the WHB

commensurate with the local heat flux and, consequently, rate of vaporization. In order to more optimally distribute feedwater, the use of a feedwater *distributor* manifold composed of a constant cross-section duct, such as a pipe, has been used in the past (Figure 1b).

Direct experimental observation of the effects of feedwater distribution within industrial-scale WHBs is currently infeasible, which motivates the use of simulations which capture, with some approximation, multiphase hydrodynamics, phase change, and heat transfer. Past work using simulation-based analysis [3] has shown that vapor distribution characteristics within WHB tube bundles are complex and vary spatially, increasing linearly with height and local heat flux. The cause for this was identified to be that the volumetric flux of steam within the tube bundle is non-uniform due to increasingly tortuous flow paths with height, referred to as “vapor traffic”, with an example simulation result shown in Figure 1c. This past work supports revisiting the standard approach to WHB design with uniform tube layouts, where non-uniform layouts could potentially to reduce vapor traffic and improve reliability at higher heat flux.

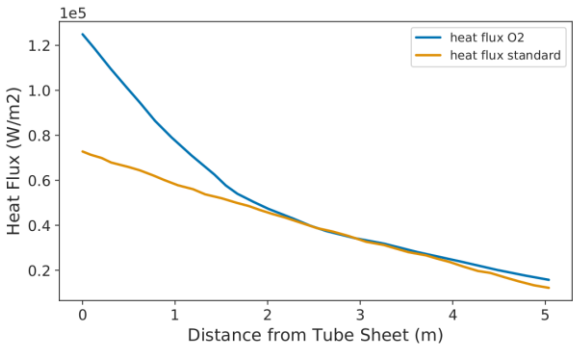

(a)

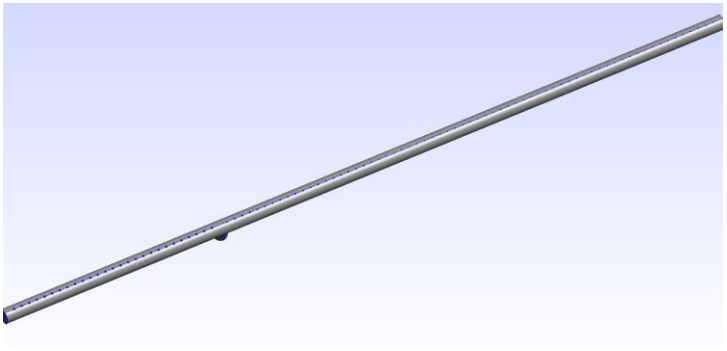

(b)

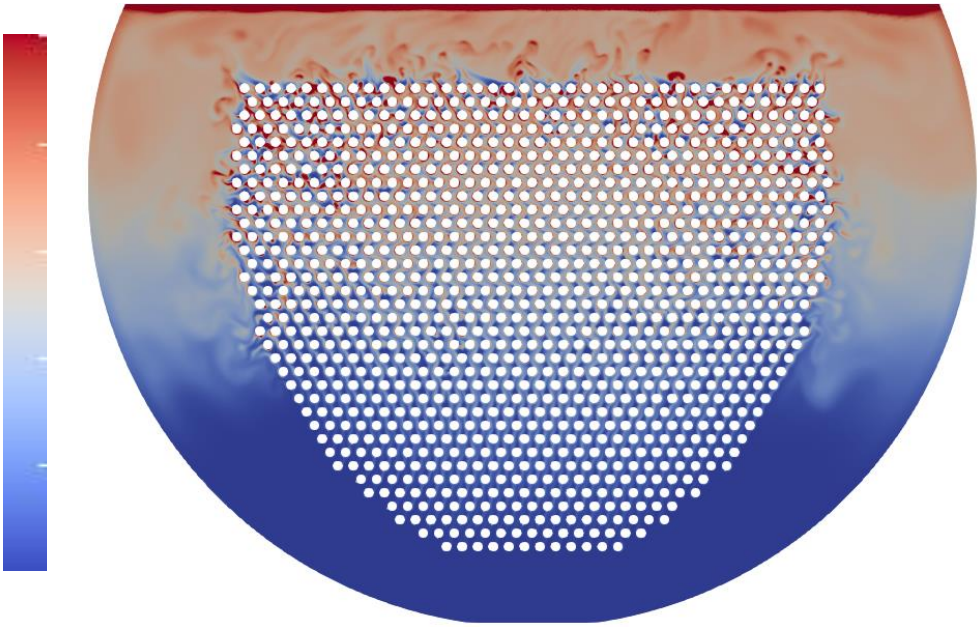

(c)

***FIGURE 1**: (a) Sample plot of heat flux versus length for a kettle-type WHB with both normal and oxygen-enrichment operating conditions, (b) schematic of pipe distributor/manifold with a single inlet and multiple outlet ports, (c) a sample 2D cross-section of multiphase multiphysics of a WHB simulations from past work [3] colored by the local steam volume fraction. Color bar range for the steam fraction is a_s=[0, 0.5].*

In this work, local feedwater distribution is investigated as another important design choice, with the hypothesis that feedwater distribution also affects vapor traffic within the WHB tube bundle. Multiphase multiphysics simulations are used to predict the effect of different rates of local feedwater injection on the multiphase hydrodynamics within a representative kettle-style WHB boiler. Simulations were performed for a range heat flux conditions, corresponding to different locations along the length of the tube bundle. The competition between convective transport and vapor distribution characteristics were investigated quantitatively, where the key attribute of vapor traffic and vapor hold-up within the tube bundle is considered [3]. Simulation approximations were made motivated by the intent of simulations to be used as a screening tool for informing design choices. Several significant observations are made regarding the effects of local feedwater injection on vapor hold-up in the tube bundle and the use of *consecutive multistage* pipe-based manifolds to optimally distribute feedwater axially to the tube bundle.

Theory and Numerical Methods

Multiphase flow models can be divided into two different general classes based on the different flow regimes they are appropriate for [4]:

- segregated flows, where macroscale interfaces exist and no continuous phase is present.
- dispersed flows, where one or more phases (fluid) are dispersed in a continuous phase (fluid).

Interface capturing multiphase models, such as the volume-of-fluid model are infeasible for large-scale transient simulation of processes that are typically present in an industrial setting including pool and convective boiling. For these processes, time/volume-averaged models such as the Euler-Lagrange [4] and Euler-Euler [4,5] models are most appropriate in that they do not require direct resolution of the interfaces between the continuous phase and the multitude of dispersed phase sub-domains.

The Euler-Euler multiphase model [4,5], also referred to as the two-fluid model (TFM) hereafter, actually refers to a class of multiphase models in which the conservation of mass, momentum, and energy equations of the continuous and dispersed phases are time/volume averaged, resulting in continuous equations scaled by the local volume fraction of each phase [5],

$$\sum_i \alpha_i = 1 = \alpha_c + \alpha_d \quad (1)$$

where a_c is the volume fraction of the continuous phase and ad is that of the dispersed phase. While the TFM has also been generalized for multiple dispersed phases, in this work we focus on two-fluid formulation with $a_c = a_w$ (continuous phase, water) and $a_d = a_s$ (dispersed phase, steam bubbles). The generalized TFM conservation of mass and momentum equations are then formulated as follows [5],

$$\frac{\partial(\rho\alpha_i)}{\partial t} + \nabla \cdot (\rho\alpha_i v_i v_i) = I_i \quad (2)$$

$$\frac{\partial(\rho_i\alpha_i v_i)}{\partial t} + \nabla \cdot (\rho_i\alpha_i v_i v_i) = -\alpha_i \nabla p + \nabla \cdot (\alpha_i \tau_i) + \alpha_i \rho_i g + M_i \quad (3)$$

where, for phase *i*, a_i is the volume fraction, r_i is phasic density, $\mathbf{v}_i$ is phasic velocity, $\mathbf{t}_i$ is phasic Newtonian stress, $\mathbf{I}_i$ is interphase mass transfer, and $\mathbf{M}_i$ is interphase momentum transfer. A single shared pressure *p* is used and interphase transfer terms for mass and momentum must be specified for an individual instance of this model. The choices of closures and approximations for these terms is extremely important and required to define a specific instance. The interphase mass transfer term includes evaporation and condensation in bulk using the Ranz-Marshall model [6], which is coupled to interphase energy transfer. In this work, the interphase momentum closures that are used include:
- drag, using the Schiller-Naumann closure [7],
- virtual mass [8],
- wall lubrication, using the Antal model [9]
- turbulent dispersion, using the Lopez-De Bertodano multiphase turbulence model [10,11]
The conservation of energy equation for the TFM can be found in ref. [5] and is not included for brevity.

Turbulence in the TFM is modeled using the combination of the k-e and multiphase turbulence models from Lopez-De Bertodano [10,11]. Given that the k-e model is most accurate for free turbulence, a wall function is used to capture boundary effects, specifically the Jayatilleke wall function [12] on tube surfaces. Insulating conditions are used on shell surfaces.

While there has been recent advancement in the area of nucleate boiling models [13,14], nucleate boiling at tube surfaces is approximated using the standard Kurul and Podowski model [13] with a fixed heat flux boundary condition. Additionally, a custom coupled inlet/outlet boundary condition was implemented which imposes steady-state conditions, w.r.t. net mass transfer, through implementation of proportional control on the inlet BFW rate, balancing BFW mass flow rate in with the steam mass flowrate out.

An open-source implementation of the TFM and supporting closures is used as provided by the OpenFOAM simulation software package (version 10) [15], which enables external verification of the presented results through the use of an open-access simulation software.

Results and Discussion

All multiphase multiphysics simulations presented were performed for an idealized two-dimensional WHB design, shown in Figure 2, with a shell diameter of 2.5 m (100 in), 28.6 mm (1 1/8 in) tubes, and 1344 tubes with triangular pitch of 44.5 mm (1 3/4 in). Simulations were performed under the following conditions:

1) Three heat fluxes with Q=15 kW/m^2, 10 kW/m^2, and 5 kW/m^2 which corresponds to a heat duty of 1811.4 kW/m, 1207.6 kW/m, and 603.8 kW/m. These heat flux conditions are meant to approximate conditions with respect to distance from the process gas inlet and are referred two as upstream, midstream, and downstream tube bundle conditions/locations.
2) Two different feedwater injection conditions are simulated: single and consecutive manifold inlets. Single-inlet conditions are approximated through a linear decay from an (axially) central injection point on the side of the WHB (shell). Consecutive manifold injection conditions are based on a linear decay from the process gas inlet side of the WHB, based on qualitative observations and semi-empirical modeling of manifold flow [16] with uniform manifold hole diameter and downstream inlet.

In all multiphase multiphysics simulations there is no expected steady-state of the velocity and phase fraction profiles and, instead, simulations were performed until developed conditions were obtained through observation of the time-averaged steam generation rate. Water level is not explicitly controlled, due to the lack of accounting for axial flow in 2D simulations. Instead the water level is allowed to increase steadily, which was found to have no significant effect on heat transfer within the tube bundle in past work [3]. It has also been assumed that there are no contaminants in the source water; it is understood that water quality is a key consideration in WHB thermal performance and reliability, and water quality will be a consideration for future evaluation.

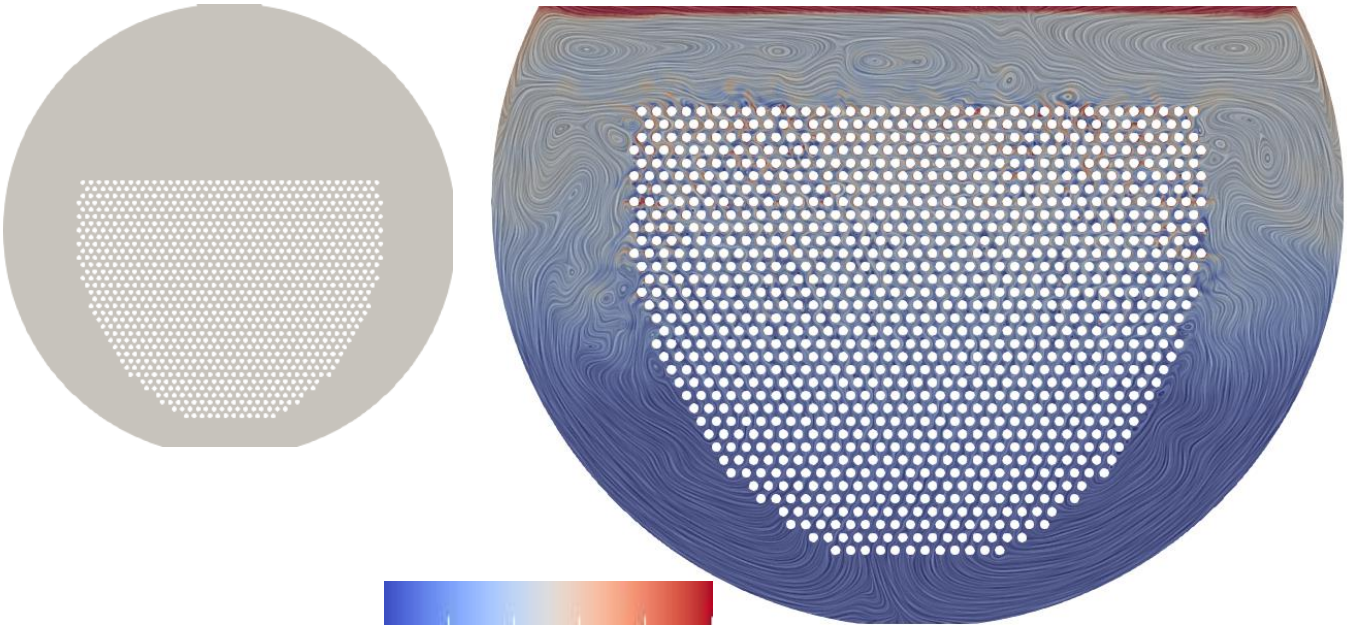

FIGURE 2*: (a) Rendering of the 2D shell-side geometry cross-section and (b) a sample 2D simulation visualization with water velocity visualized using the line integral convolution method [17], indicating the local velocity direction and colored by the local steam volume fraction. Color bar range is from* a_s*=[0, 0.5].*

Additionally, single-phase computational fluid dynamics simulations are performed to show the effects of variable port size on feedwater distribution using a simple pipe manifold. This approach, so-called "multistage" manifolds, are shown to enable more precise control of feedwater distribution to be commensurate with local heat flux (as shown in Figure 1a).

Single-inlet versus manifold feedwater injection

In the first part of the study, multiphase multiphysics simulations were performed for the reference WHB for two different feedwater injection conditions: single-inlet versus manifold designs. Given that the effects of axial flow are not captured in 2D simulations, a simple linear decay approximation was used based on intuitive distribution of feedwater associated with each design. This refers to the amount of *excess* feedwater provided to the tube bundle locally, proportional to the minimum flowrate required to conserve mass, which is equal to the amount of steam vapor (by mass) locally generated.

For the single-inlet design, injection was performed on the right side of the shell (3 o'clock position facing the upstream tubesheet) with maximum feedrate of 150% (1.5 times the amount of steam locally generated) at the center of the WHB, corresponding to the 10 kW/m^2 heat flux condition. Both upstream and downstream cases, corresponding to heat fluxes of 15 kW/m^2 and 5 kW/m^2 were assumed to have feedrates of 100% (equal to the amount of steam locally generated). The rationale for this is intuitive, the majority of feedwater flowrate will be in the vicinity of the injection point for a single-point injection design, with redistribution of feedwater resulting from the natural recirculatory flow within the shell-side of the WHB which must have a significant axial component under these conditions.

For the manifold-inlet design, injection was performed at the bottom of the tubesheet, which is due to structural considerations where the manifold/pipe rests either on supports or within baffle cut-outs. This allows for adequately structural support and placement of a pipe-type manifold so that it does not interfere with blowdown activities. The distribution of feedwater within a manifold is not as intuitive as for a single-point injection in that there is a competition between *turning loss* and *frictional loss* of flow within the manifold and through its ports. This affects local port flowrate such that it is highly non-uniform under many conditions [16] and thus volumetric flow distribution throughout the manifold.

Turning loss refers to the inertia of the flow in the axial direction of the manifold which must be overcome to redirect a portion of that flow through the nearest manifold port. Frictional loss is that associated with the hydrodynamic diameter, length, and other hydrodynamic effects of flow through the port. For a manifold with uniform port size, turning loss decreases with distance from the manifold inlet due to the reduction of volumetric flow, and thus velocity/inertia, resulting in volumetric flow from each port increasing with distance (from the inlet). This will be discussed in more detail in the next section, with this being the justification for the feedrate conditions increasing with distance from

the manifold inlet, which is assumed to be at the downstream end of the WHB. Thus the maximum feedrate of 150% (1.5 times the amount of steam locally generated) is used at the process gas inlet side of the WHB with heat flux of 15 kW/m^2, 125% feedrate in the center of the WHB with heat flux of 10 kW/m^2, and the outlet side of the WHB is assumed to have a feedrate of 100% (equal to the amount of steam locally generated) with heat flux of 5 kW/m^2.

Figures 3 show a visualizations of the instantaneous steam vapor distribution within the tube bundle for the single-inlet case for midstream heat flux case (10 kW/m^2) with over-injection of 150%. For the upstream (15 kW/m^2) and downstream (5 kW/m^2) cases, both not shown (refer to Figures 2 and 4 from ref. [3]), the water level above the tube bundle was maintained at approximately 10-15cm, but for the midstream case (10 kW/m^2) the water level steadily increases due to over-injection and the simulations not accounting for axial recirculation. The steam distribution characteristics around and within the tube bundle have several key features and regions as were discussed in previous work [3]. Summarizing here, within the tube bundle is an increase of the local steam fraction in the vertical direction from bottom-to-top due to the buoyancy-driven convection of steam from lower tubes combining with steam locally generated at the tube surfaces. Thus the volumetric flux of steam increases significantly with height in the tube bundle, along with a slight divergence from the centerline due to the specific configuration used for the reference WHB. The one noticeable deviation of the recirculation profile for the side inlet case is the slight asymmetry of the steam fraction, compared to injection from below (Figure 1b).

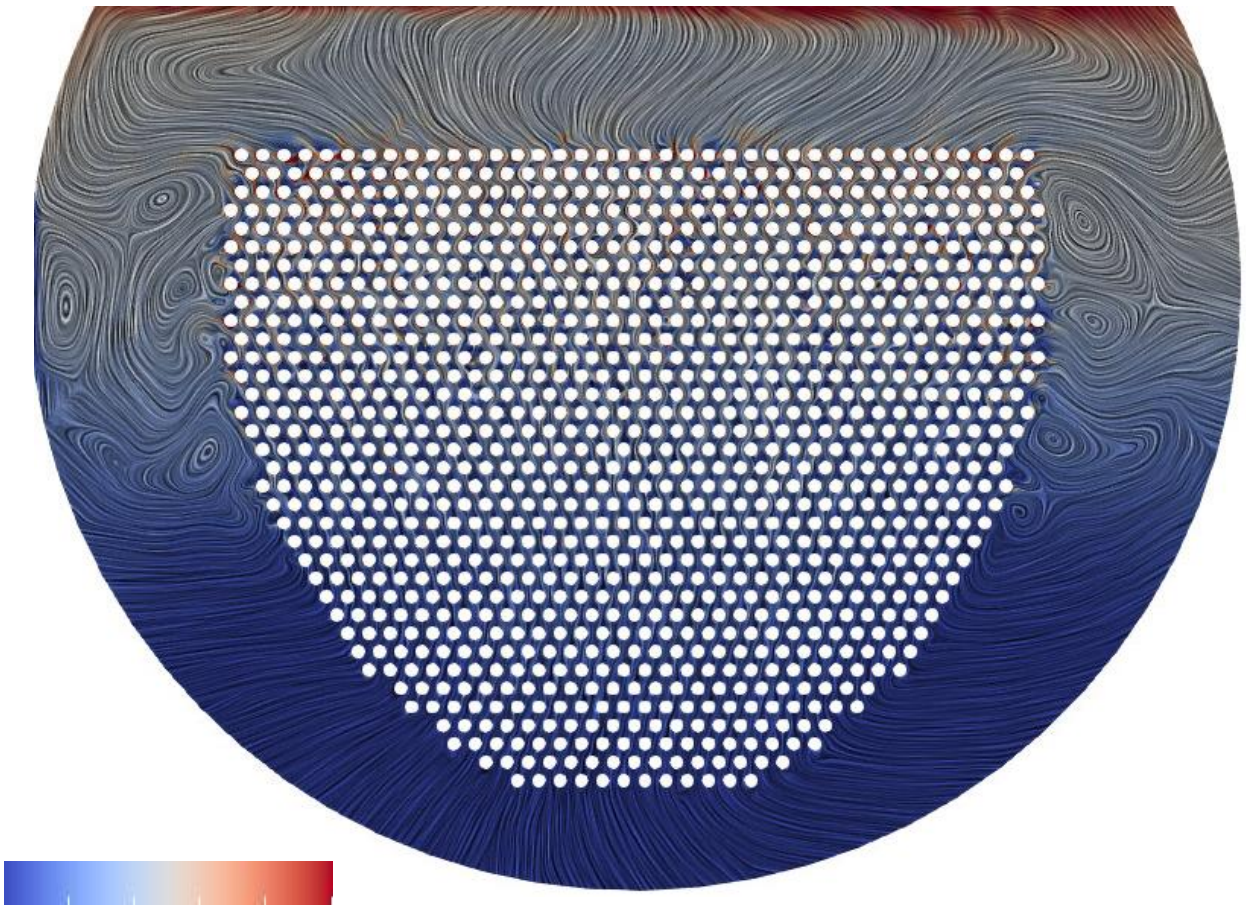

FIGURE 3: *Visualizations of vapor fraction (color) and water velocity direction (LICs) for the midstream side injection case. Color bar range is from* α_s*=[0, 0.5].*

For the upstream case, where the heat flux is greatest, the amount of steam hold-up is qualitatively larger than for the midstream and downstream cases. As shown in past work [3], this can be quantified through computing the horizontal average steam volume fraction. Figure 4a shows both the time-averaged feedrates for each of the cases (upstream, midstream, and downstream) along with the average steam fraction versus height for 100% feedrate (Figure 4b), and a comparison of the midstream case with feedrates of both 150% and 100% (Figure 4c). As is expected, feedrates are proportional to heat flux and, thus, non-uniform throughout the WHB based on the axial heat flux variation (Figure 1a). For all cases, the steam fraction profiles show an approximately linearly increasing relationship of steam fraction with height and increase in slope as heat flux increases. Comparing midstream simulations, the over-injection of feedwater is not shown to appreciably affect for the simulated tube bundle configuration. This is intuitive in that side injection does not distribute feedwater *directly* to the bottom of the tube bundle and, instead, simply increases the overall amount of water available for recirculation.

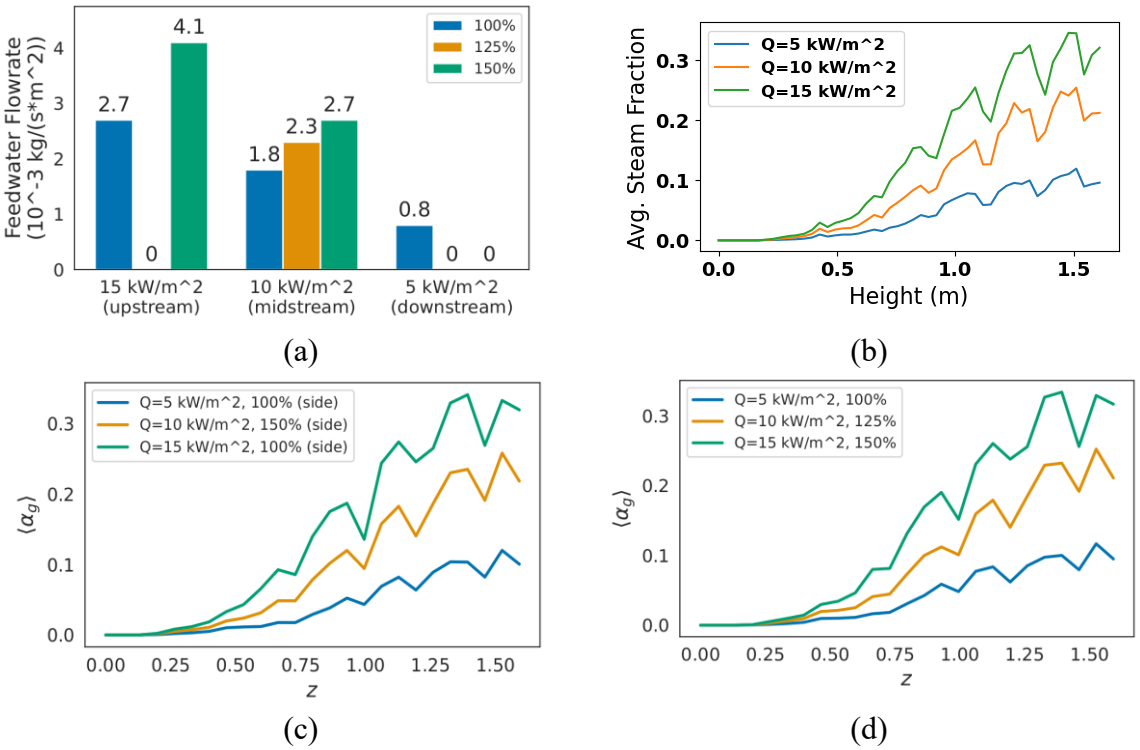

FIGURE 4: *Plots of (a) time-averaged feedwater flowrates (zero values correspond to no data/simulation); horizontally averaged steam fraction for (b) ref. [3] simulations with 100% feedrate (no over-injection), (c) single-inlet simulations, and (d) manifold inlet simulations.*

Figures 5a-b shows visualizations of the instantaneous steam vapor distribution within the tube bundle for the manifold inlet design where the over-injection is 150% and 125% for the upstream and midstream cases, respectively. The downstream case has the same injection rate of 100% and has a similar steam vapor fraction profile as in past work (Figure 2a of ref. [3]). Similar to the midstream case from the previous set of simulations, there is no significant change in the vapor hold-up for both over-injection cases compared to 100% injection (Figures 2b-c of ref. [4]). This is quantitatively shown in Figure 4c. The lack of an effect of over-injection in steam hold-up is not intuitive without analyzing the flow profile through the tube bundle, shown in Figure 3. While the flow direction in the lower portion of the tube bundle is essentially unidirectional, there is a slight bias away from the centerline. The main driving force for both convection of water into the tube bundle and convection of steam out of the tube bundle is buoyancy force. As with a thermosiphon-type WHB, this corresponds to natural convective boiling which is enhanced through the design of the shell-side of the boiler, for the kettle-type design. However, as was described in past work [3], this natural convection of water and steam within the tube bundle is strongly affected by vapor "traffic", where there is a significant difference between the volumetric flux of steam and water between the lower and upper tubes in the tube bundle. However, over-injection of feedwater from below the tube bundle is found to not contribute to improve steam/water convection in the upper and central region where steam hold-up is greatest.

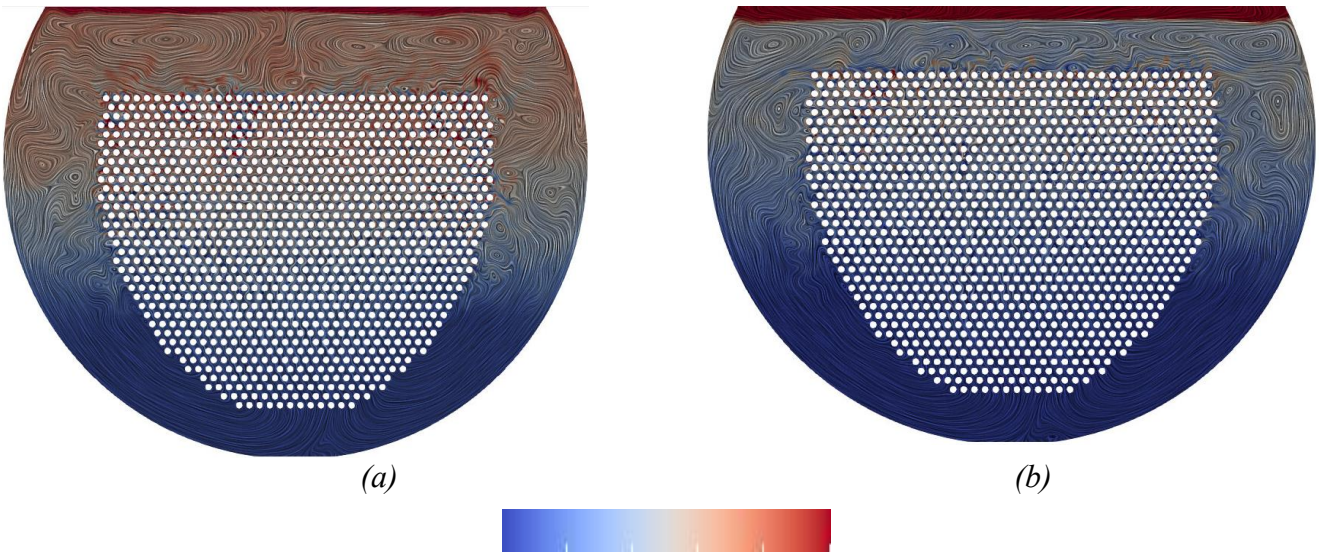

FIGURE 5: *Visualizations of vapor fraction (color) and water velocity direction (lines) for the (a) upstream and (b) midstream manifold injection cases. Color bar range is from* a_s*=[0, 0.5].*

For both over-injection cases, the feedwater injection directly below the tube bundle does provide some additional potential for increasing the driving force for overall convective flow through the tube bundle. However, the uniform layout of tubes along with the bias of vapor/liquid flow away from the centerline of the tube bundle dissipates this additional inertia of the injected feedwater and the corresponding increase in the water fraction of volumetric flux entering the tube bundle. It is the same effect that causes this vapor hold-up that disperses the additional feedwater that is injected, that is, the increasingly tortuous paths for water/steam to flow due to the vapor traffic from lower tubes. These observations further support the need for the design of non-uniform tube layouts to accommodate steam traffic, which could also be designed to enable over-injection flowrate to be used to further reduce steam hold-up through forced-convection.

Manifold-based feedwater distributor design analysis

Given the motivation to distribute feedwater non-uniformly along the length of the tube bundle within a WHBs, the use of a pipe manifold or feedwater distributor has been used for a small set of existing units. Flow distribution in manifolds has been the focus of much past study, with theory-based flow distribution models for both consequential and bifurcation manifold types [16] providing relatively accurate models for manifold design. Consecutive-type (pipe or duct-based) manifolds are frequently used, due to their compactness and simplicity of fabrication, where the manifold typically has constant cross-sectional area with multiple ports (holes). The current standard theory-based model for manifold flow is as follows [16],

$$\frac{1}{\rho}\frac{dP}{dX} + \frac{f}{2D}W^2 + \frac{2-\beta}{2}\frac{dW^2}{dX} = 0$$

where X is the axial length or distance from the manifold inlet, P is axially varying manifold pressure, W is axial velocity, D the hydraulic diameter of the manifold, and β the average velocity ratio (port over manifold). This model is then discretized, which enables the incorporation of ports and numerical solution,

$$\Delta P + \frac{\rho f}{2D}W^2\Delta X + \frac{(2-\beta)\rho}{2}\Delta W^2 = 0$$

which requires additional empirically-determined friction and recovery factors in order to be solved either analytically or numerically.

The need for additional empirical information, particularly about frictional losses through the ports, motivates the use of numerical solutions of more accurate continuum models, typically referred to as computational fluid dynamics. However, analysis of this simplified standard model provides some insight into basic design principles for consecutive manifolds, which is described in detail in Sections 4-5 of ref. [16], showing that the flow and pressure profiles predicted by this model depend highly on the friction and pressure recovery factors used to inform it. For example, flow through each port of the manifold can be shown to be approximated by a modification of Bernoulli's equation to include a contribution from turning loss,

$$P - P_c = \rho\left(1 + C_f + f_c\frac{l_c}{d_{ch}}\right)\frac{U_c^2}{2} = \rho\zeta\frac{U_c^2}{2}$$

where C_f and f_c are empirically determined coefficients of turning and frictional loss, with l_c and d_{ch} being the length and diameter of ports. A few important considerations for interpreting this relationship are that:

- the pressure within the manifold increases with distance from the inlet as axial velocity decreases, corresponding to a transition of momentum flux (stress) from convective to hydrostatic,
- the axial velocity within the manifold also decreases with distance from the inlet, corresponding to a decrease in the turning loss due to the reduced axial momentum.

The net result is that volumetric flow through ports of uniform cross-sectional area *increases* with distance from the manifold inlet. Thus, assuming a feasibility constraint of *constant* manifold cross-sectional area (a standard pipe or other duct), variation of port diameter, placement, and manifold inlet location provides a large design space for customizing flow distribution.

Within the context of the non-uniform heat transfer and rate of vaporization present in WHBs (see Figure 1a) and the intuitive understanding that feedwater should be non-uniformly distributed along the tube bundle, there is motivation to develop manifold-based distributor designs which optimally distribute feedwater proportional to local heat flux within the tube bundle. A simulation-based study

was performed using the steady-state Reynolds-averaged Navier-Stokes model [18] with the k-ω SST turbulence model [19] to understand flow distribution properties for a sample WHB feedwater distribution manifold. A manifold length of 4.7m was used with an inlet location of 1.5m from the downstream tubesheet, an inner diameter of 90mm, and ports of various inner diameters (3-9 mm) spaced 50mm from each other along the manifold length, see Figure 1b.

Steady-state simulations were performed initially for a range of port diameters ranging from 3mm to 9mm, with a total number of 90-93 ports with an inlet volumetric flowrate of 10^4 kg/hr at 145 C. Figures 6a-c show volumetric flow profiles for each of these cases, compared to an ideal uniform flow distribution. Several observations can be made regarding the feedwater volumetric flowrate resulting from this manifold design:

- it becomes more uniform with decreasing port size,
- it increases with distance from the manifold inlet nonlinearly,
- it deviates from both of these trends in the entrance region close to the manifold inlet.

The first and second observations are consistent with the standard model approximation for consecutive manifold flow [16]. However, entrance region effects are not predicted by the standard model and the use of computational fluid dynamics to capture these entrance effects is clearly needed. The cause of this deviation of flow from that predicted by the standard model is due to the *redirection* of feedwater from the inlet (radial/vertical) into the manifold (axial). Thus, turning loss is negligible for the ports directly across from the manifold inlet.

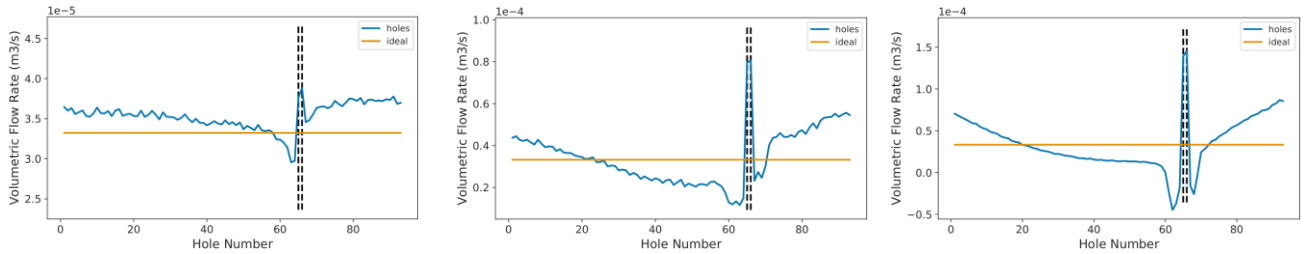

(a) *d=3mm* (b) *d=6mm* (c) *d=9mm*

FIGURE 6*: Plots of volumetric flowrate versus port number, labelled from 0-96 starting from the upstream tubesheet end of the distributor. Ideal/uniform flowrate is shown corresponding to the total volumetric feedwater flowrate divided by the number of ports. Vertical dashed lines identify ports directly opposite to the manifold inlet.*

The first design change attempted in order to mitigate the lack of significant turning loss of inlet-adjacent ports was to simply remove these ports. Visualization of the feedwater velocity field in the vicinity of the manifold inlet is shown in Figure 7a for a sample case. By removing ports in regions of the distributor manifold in which redirection of the inlet flow occurs, more precise control of feedwater distribution can be achieved. Simulations were then performed for a modified distributor design with port diameter of 6mm, as shown in Figures 7b. Simulation results show that the entrance effects are not

completely mitigated, but there is significant improvement compared to the corresponding case with inlet-adjacent ports included (Figure 6b). However, the additional challenge of biasing feedwater distribution to the inlet side of the tube bundle is not addressed. Two possible design changes could be explored to more yield a more optimal feedwater distribution: (i) relocation of the feedwater inlet farther downstream or (ii) the use of different "stages" of port diameters. The latter was chosen in this work, based on the design paradigm that decreasing port diameter increases frictional losses.

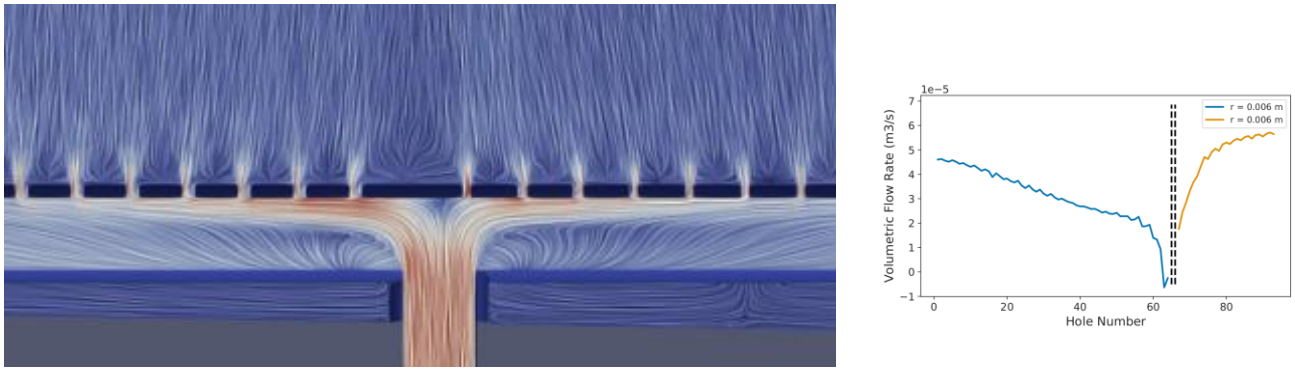

FIGURE 7: *(a) Simulation visualizations of the feedwater velocity and direction in the inlet region of the distributor and (b) plot of volumetric flowrate versus port number for the "blocked" distributor.*

A two-stage manifold design was simulated with 6mm ports on the upstream stage, 3mm ports on the downstream stage, and with two ports adjacent from the feedwater inlet not included. Figure 8 shows the volumetric flowrate profile with a representative WHB heat flux profile superimposed for reference. The combination of blocking-off ports adjacent to the feedwater inlet and using an increased port diameter for the upstream stage of the distributor results in a relatively optimal feedwater distribution to the WHB tube bundle, based on the typical heat flux profile.

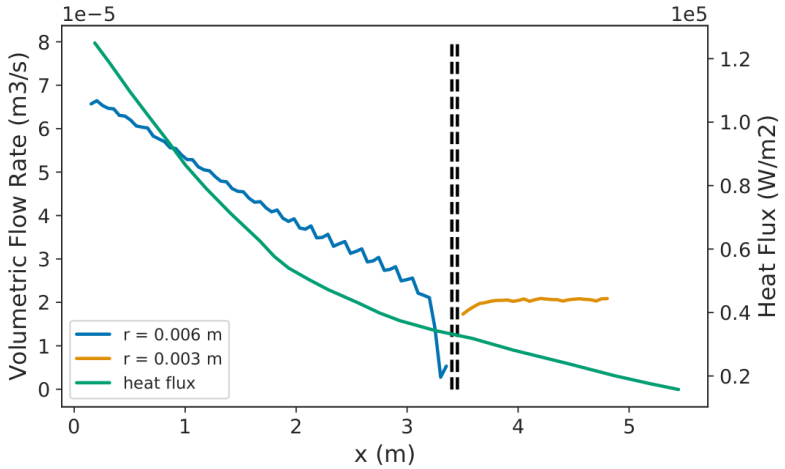

FIGURE 8: *Plot of volumetric flowrate versus port number for the multistage distributor.*

Given the high accuracy and relatively low computational costs of single-phase CFD simulations, assuming that they are performed using best practices, motivates there use for feedwater distributor design compared to the current standard theoretically-informed approach described previously [16]. CFD simulations do not require additional empirically-determined information regarding port frictional losses and enable a broad design space to be explored including multiple port sizes, geometrical placement, and feedwater inlet locations which are best for a specific WHB design and potential geometric limitations due to baffle and manway placement.

Conclusion

As modern WHBs within SRUs are being used to generate steam at higher pressures than in the past, corresponding to higher heat loads for new and legacy units, the need for new and retrofit designs to improve reliability and longevity is clearly motivated. Direct experimental observation of existing conditions within the two-phase shell-side of the WHB is infeasible, which motivates the use of simulations which capture, with some approximation, multiphase hydrodynamics, phase change, and heat transfer. Recent studies using simulation-based analysis [3] has shown that vapor distribution characteristics within WHB tube bundles are complex and vary spatially, increasing linearly with height and local heat flux.

In this work local feedwater distribution along the length of the tube bundle was investigated along with the use of consecutive manifolds to achieve desired feedwater distributions, again using simulations for design. Simulations were performed for a range of heat flux conditions, corresponding to different locations along the length of the tube bundle and it was found that local vaporization rates vary greatly. The effects of local feedwater *over-injection* on vapor hold-up in the tube bundle was also investigated finding that, for the reference WHB design, over-injection did not have a significant effect on reducing vapor hold-up. However, further study is needed for different tube bundle geometries and spacings.

A second simulation-based study was performed analyzing flow in consecutive manifold-based distributors. The effect of feedwater inlet location and port size was studied, showing that the use of larger diameters results in significant increase in volumetric flowrate in ports with increasing distance from the manifold inlet. However, ports in the vicinity of the manifold inlet have extremely high volumetric flowrates, resulting from the low turning losses of flow adjacent to the manifold inlet. Blocking or removal of ports from this region was found to significantly reduce this issue.

The concept of “multistage” distributors was introduced, that is, the use of different port diameters to impose feedwater flow distributions commensurate with local heat flux. Larger port diameters in regions of the distributor adjacent to high heat flux regions of the tube bundle, versus smaller port diameters in low heat flux regions, was found to result in commensurate feedwater distribution. Overall, the use of single-phase CFD enables simulation-based evaluation of a large design space of manifold-based feedwater distributors. Consequently, the use of customized distributors for new and

legacy WHBs could potential increase their reliability and longevity through minimizing axial feedwater flows.

References

1. Nasato E, Misale-Lyttle D, Huffmaster M, Examining the Impact of Waste Heat Boiler Design and Operation on waste heat boiler Reliability, Sulphur 2015, Toronto, Canada, November 2015
2. Knight, W P, Evaluate waste heat steam generators, Hydrocarbon Processing, 57, 1978
3. Nasato E, Treeratanaphitak T, Abukhdeir N M,Simulation-based Analysis of Vapor Distribution and Liquid Recirculation in Kettle-type Waste Heat Boilers, SulGas 2023, Mumbai, India, February 2023
4. Cheung D C, Tu J, Yeoh G H, Multiphase Flow Analysis Using Population Balance Modeling: Bubbles, Drops and Particles, Netherlands: Elsevier Science, 2013.
5. Hibiki T, Ishii M, Thermo-fluid Dynamics of Two-Phase Flow, Germany:Springer, 2006.
6. Charlesworth D H and Marshall W R, Evaporation from drops containing dissolved solids, AIChE Journal, 6(1), 1960 .
7. Naumann Z and Schiller L, A drag coefficient correlation, Z Ver Deutsch Ing, 77, 1935.
8. Drew D, Cheng L, and Lahey R T, The analysis of virtual mass effects in two-phase flow, International Journal of Multiphase Flow, 5(4), 1979.
9. Antal S P, Lahey R T and Flaherty J E, Analysis of phase distribution in fully developed laminar bubbly two-phase flow, International Journal of Multiphase Flow, 17(5), 1991.
10. Lopez-de Bertodano M, Turbulent bubbly two-phase flow in a triangular duct. PhD Thesis, Rensselaer Polytechnic Institution, 1992.
11. Lopez-de Bertodano M, Lahey R T, and Jones O C, Turbulent bubbly two-phase flow data in a triangular duct, Nuclear Engineering and Design, 146(1-3), 1994.
12. Jayatilleke C LV, The influence of Prandtl number and surface roughness on the resistance of the laminar sub-layer to momentum and heat transfer. Imperial College of Science and Technology, 1966.
13. Kurul N, Multidimensional effects in two-phase flow including phase change. Rensselaer Polytechnic Institute, 1990.
14. Lin Y C et al, Assessment of Nucleation Boiling Models and Improvement by the Chen Correlation for Two-fluid Model CFD, International Journal of Heat and Mass Transfer, 175, 2021.
15. https://openfoam.org/version/10/
16. Wang J, Theory of flow distribution in manifolds, Chemical Engineering Journal, 168, 2011.
17. Stalling D and Hege H C. Fast and resolution independent line integral convolution, Proceedings of the 22nd Annual Conference on Computer Graphics and Interactive Techniques, 1995.
18. Bird R B, Lightfoot E N, Stewart W E, Transport Phenomena, United Kingdom: Wiley, 2007.
19. Menter F R. Improved two-equation k-omega turbulence models for aerodynamic flows. 1992.